JACS
JOURNAL OF THE AMERICAN CHEMICAL SOCIETY



pubs.acs.org/JACS
Article

# Molecular Tweezers Block the Functional Pore of a Protein Machine

Abbna Kirupakaran,[§] Johannes van den Boom,[§] Mike Blueggel, Christine Beuck, Felix Niemeyer, Matthias Hayduk, Jan Balszuweit, Peter Bayer, Jens Voskuhl, Hemmo Meyer,* and Thomas Schrader*

Cite This: J. Am. Chem. Soc. 2025, 147, 16836−16849

Read Online

ACCESS | Metrics & More | Article Recommendations | Supporting Information

**ABSTRACT:** We present symmetric multivalent tweezers as the first class of supramolecular elements designed to cover and functionally block a protein pore. As a model, we chose the enzyme p97, a hexameric AAA-ATPase that unfolds or segregates substrate proteins by threading them through a pore and channel at the center of the symmetric p97 hexamer fueled by ATP hydrolysis. In a rational design approach, we developed a new class of p97 inhibitors, guided by molecular modeling. These dock onto lysine residues at the entry of the pore via appropriately positioned molecular tweezers. Ligand binding was accompanied by induction of fluorescence of the built-in binding sensitive luminophores which served as a sensor for affinity determination. We further confirmed specific interaction with p97 as well as concomitant inhibition of ATPase activity and protein substrate unfolding using an array of biophysical methods and state-of-the art biochemical assays. Specific binding was also validated by mutagenesis, demonstrating that inhibition of p97 function was mediated by blocking the pore entrance. Especially $C_3$-symmetric multivalent tweezers potently inhibited ATPase activity and protein substrate processing consistent with the symmetry of the docking site. Our data independently confirm substrate threading as a mechanism for protein unfolding by p97 and highlight multivalent tweezers as a supramolecular strategy to target pores in various proteins. Since p97 and related protein machines are vital for protein quality control and cell survival, the new pore binders may open a new approach to combat diseases and be employed in drug discovery.

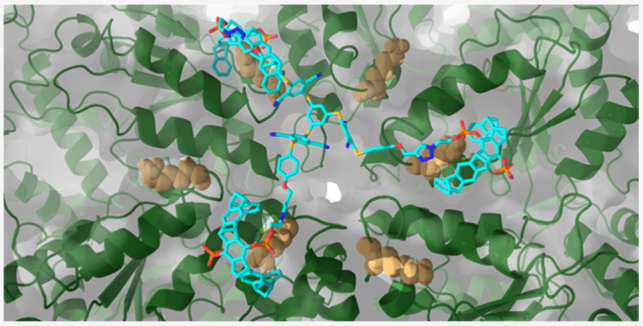

## INTRODUCTION

In recent years, Supramolecular Protein Chemistry has begun to explore not only well-defined active sites (classical medicinal chemistry), but also the protein surface (PPIs) and elements of various topology such as clefts, loops and secondary structures. A deepened understanding and theoretical treatment of all underlying noncovalent interactions in combination with the full repertoire of Organic Synthesis allows us nowadays to design artificial binders for biomacromolecules which are not found in Nature. These may be further developed and optimized as new mechanistic tools or for a deliberate interference with selected protein functions, with a potential for diagnostic and therapeutic applications.

Small molecules, larger oligomeric assemblies and even polymers have been designed for their natural protein target or imprinted by their natural protein template. An increasing number of 3D structures between proteins and complementary supramolecular ligands has been accumulated (X-ray, NMR, Cryo-EM), strongly supported by advanced calculations (MD simulations and QM/MM calculations).

Among others, supramolecular binders have been developed for $\alpha$-helices[1] and $\beta$-sheets,[2,3] N- and C-termini,[4] deep clefts[5] and large protein interfaces.[6] They could be exploited to interfere with pathologic protein aggregation,[7] trigger protein dimerization[8] and stabilize or inhibit critical contacts to other partner proteins.[9] Allosteric effects were used to study conformational coupling of protein machines,[10] or to inhibit enzymatic activity by preventing substrate access to the active site.[11]

However, until today the rational design of specific protein surface ligands remains highly challenging, and most inhibitors of (effectors for) protein−protein interactions have been derived from extensive screens in compound libraries. Functional elements with a high degree of symmetry on the protein offer the opportunity to create a multivalent architecture from single binders.

A prominent example for symmetric proteins are hexameric ATPases Associated with diverse Activities plus (AAA+) proteins that have a 6-fold symmetry around a central channel.[12] AAA-ATPases form a large class of enzymes that use the energy of ATP hydrolysis to structurally remodel substrate molecules. We focused on the conserved and essential AAA+ -type ATPase p97 (also called VCP for

Received: October 30, 2024
Revised: March 18, 2025
Accepted: March 20, 2025
Published: May 12, 2025





https://doi.org/10.1021/jacs.4c15288
J. Am. Chem. Soc. 2025, 147, 16836−16849

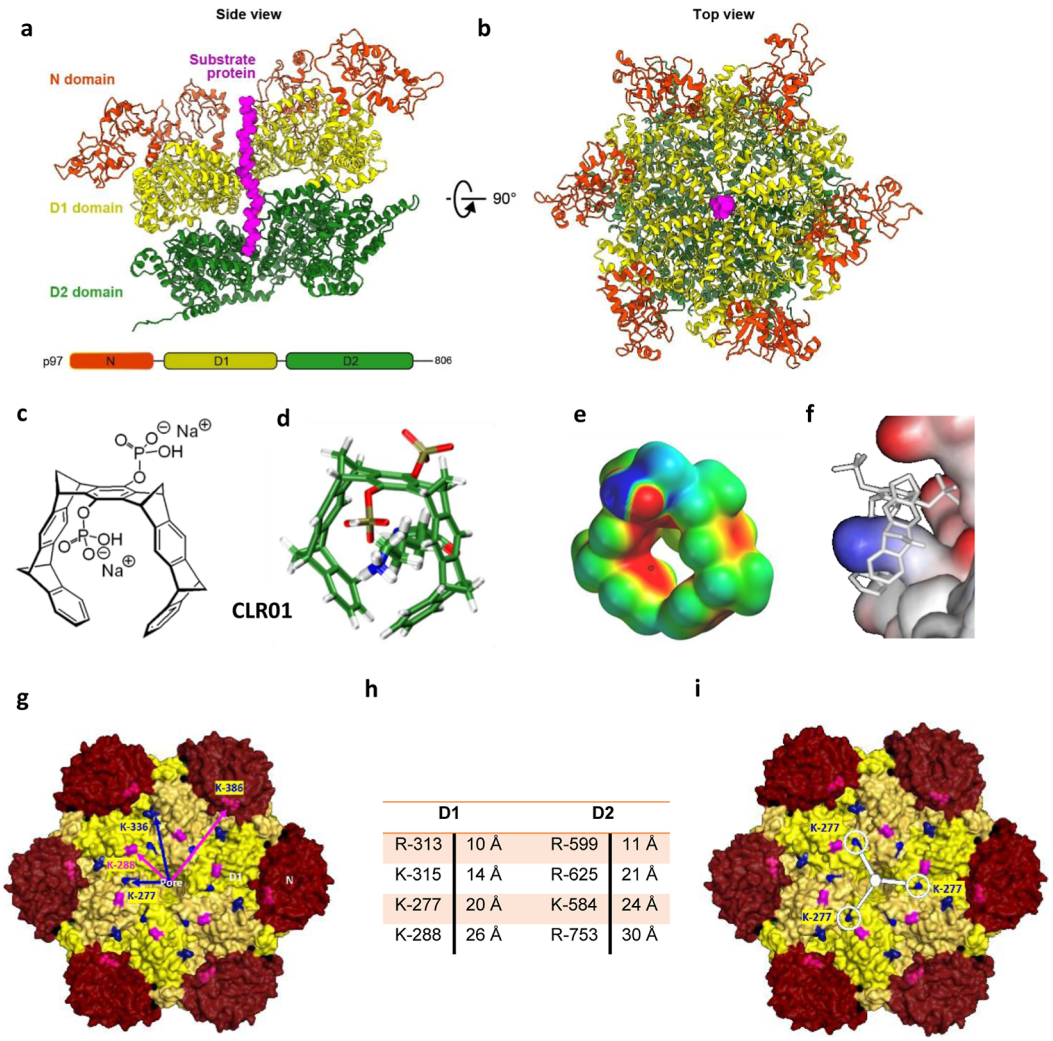


| D1 | | D2 | |
|---|---|---|---|
| R-313 | 10 Å | R-599 | 11 Å |
| K-315 | 14 Å | R-625 | 21 Å |
| K-277 | 20 Å | K-584 | 24 Å |
| K-288 | 26 Å | R-753 | 30 Å |

**Figure 1.** Segregase p97 with its central pore and molecular lysine tweezers as potential supramolecular pore plugs—design concept.

valosin-containing protein). p97 is critically involved in a large number of diverse cellular signaling and stress response pathways including DNA replication and damage repair, ER-associated degradation and autophagy that ensure cell survival and homeostasis.[13] On the molecular level, p97 mobilizes and unfolds ubiquitin-modified proteins for subsequent degradation in the proteasome.[14] Alternatively, it segregates protein complexes in a ubiquitin-independent manner, for example during activation of protein phosphatase-1 (PP1).[15] For its diverse functions, p97 cooperates with alternative substrate adapters and is modulated with a multitude of additional binding proteins.[16,17] Preclinical studies in mice demonstrated p97 to be a valuable drug target in certain cancers,[18] as well as for viral infections including SARS-CoV-2.[19,20] The first clinical trial of an inhibitory compound failed due to unfavorable pharmacokinetics and side effects (NCT02243917). However, an approved and repurposed drug with anticancer activity was recently shown to act through inhibiting p97 activity[21] confirming the high potential of targeting p97. On the other hand, missense mutations in p97 cause a dominantly inherited neuromuscular degenerative disease in humans termed multisystem proteinopathy-1 (MSP-1) featuring elements such as Parkinsonism, inclusion body myopathy, amyotrophic lateral sclerosis and frontotemporal dementia.[22]

The p97 protein contains two AAA-ATPase domains, D1 and D2 that form two stacked hexameric rings with a central channel and pores on both ends (Figure 1a).[23] The regulatory N-domains are positioned at the periphery of the D1 ring and undergo dynamic up-and-down movements controlled by adapter binding and ATP hydrolysis in D1.[24] For protein unfolding or protein complex segregation, substrate proteins bind via a substrate adapter at the ND1 side of the p97 hexamer and are subsequently inserted into the D1 pore. The p97 subunits are in a spiral staircase configuration in which aromatic residues in the pore loops engage in nonsequence-specific interactions with the substrate peptide backbone. Substrate threading occurs in a sequential hand-overhand mechanism in which ATP hydrolysis in the subunit at the bottom of the p97 spiral results in a discontinuity as it triggers the detachment of this subunit from the spiral and induces its reattachment to the substrate peptide at the top. Thus, the peptide is pulled through the pore with the progression of nucleotide binding and hydrolysis around the ring, which drives protein unfolding and segregation from potential binding partners (Figure 1b).[24−26]

Whereas substrate threading is mostly driven by ATP hydrolysis in the D2 domain adopting a staircase configuration, the configuration of the D1 domain ring and to what degree it contributes to the substrate threading mechanism has


https://doi.org/10.1021/jacs.4c15288
J. Am. Chem. Soc. 2025, 147, 16836−16849

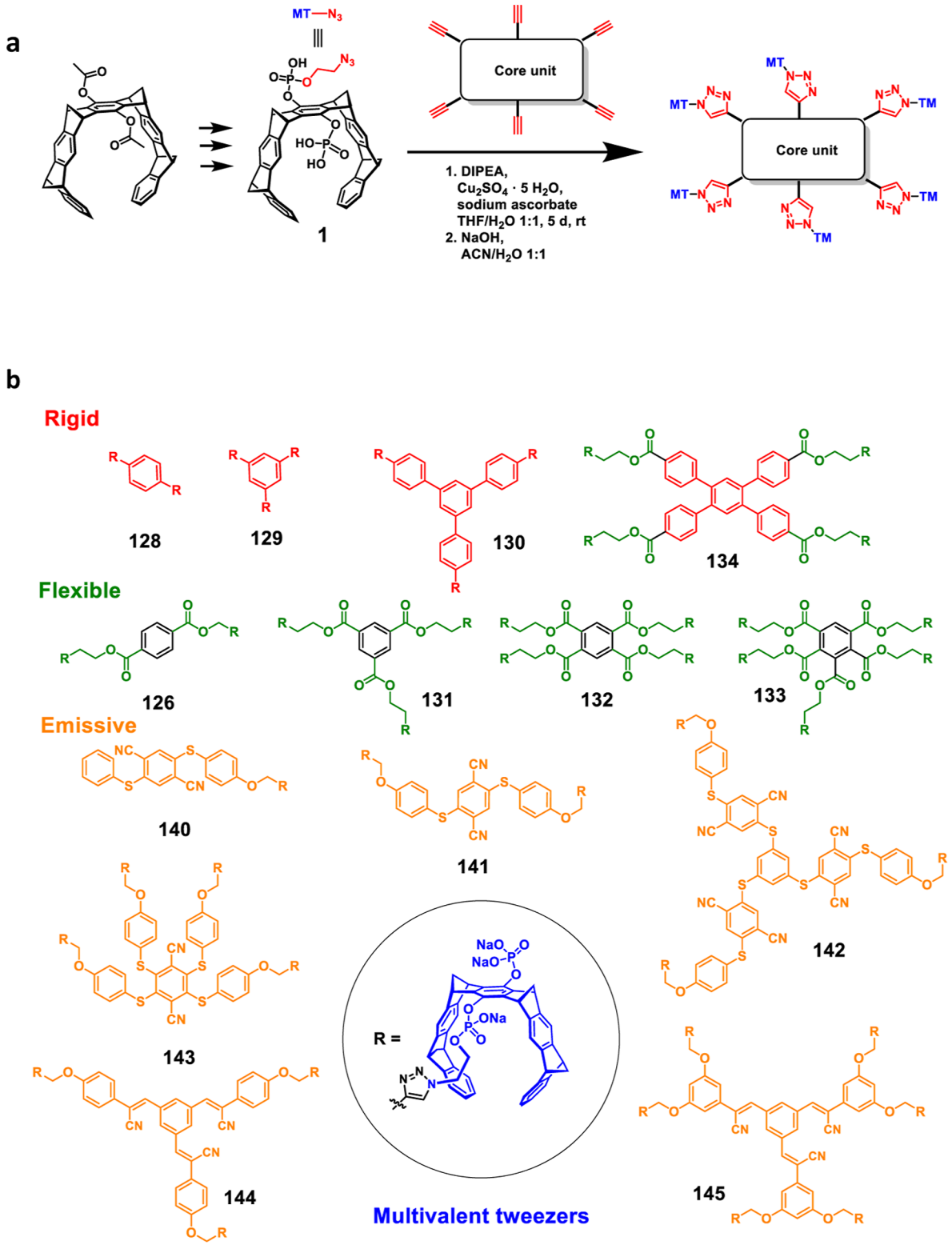


**Figure 2.** continued



https://doi.org/10.1021/jacs.4c15288
J. Am. Chem. Soc. 2025, 147, 16836−16849

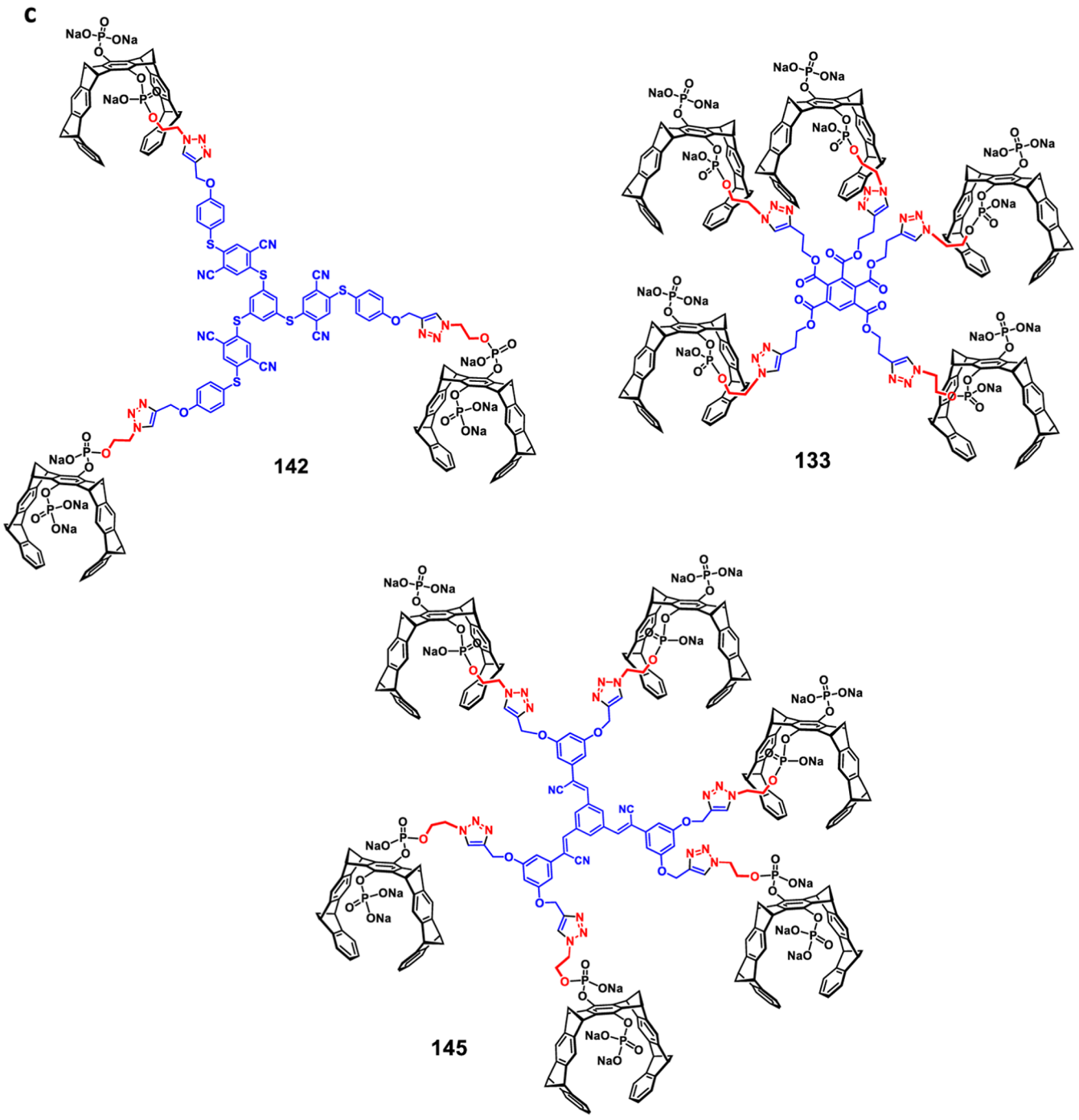


**Figure 2.** Synthesis of different classes of multivalent tweezers with a high degree of symmetry.

remained controversial. To clarify this question, it would be most helpful if synthetic receptor molecules could be designed to bind and obstruct the D1 entry pore. With the established functional assays and sensors at hand, such a compound class would open up a unique opportunity to study the nature of D1 function and establish a proof-of-concept for its modulation. This report presents the first class of supramolecular multivalent pore plugs for the D1 pore and describes their interaction with p97.

For a rational design, the noncovalent coverage of a protein pore on a flat surface poses a great challenge, because there are no obvious anchor points.[27] In this respect, the 6-fold symmetry of the self-assembled D1 and D2 domains in p97 provides a handle to the supramolecular chemist: each amino acid occurs six times on the D1 surface, with an equal distance from the pore and equal distances from the others. If a highly selective amino acid binder could be attached to a symmetric core unit, this construct could be placed exactly over the pore and undergo six simultaneous interactions with the symmetrically arranged amino acid counterparts. Such a binding mode would be superior to all other potential multivalent ligand/surface interactions, since those lack the high degree of symmetry.

In 2005, we discovered a specific/highly selective binder for the amino acids arginine and lysine, which rejects all other amino acids because it employs a unique binding mechanism.[28]



https://doi.org/10.1021/jacs.4c15288
J. Am. Chem. Soc. 2025, 147, 16836−16849

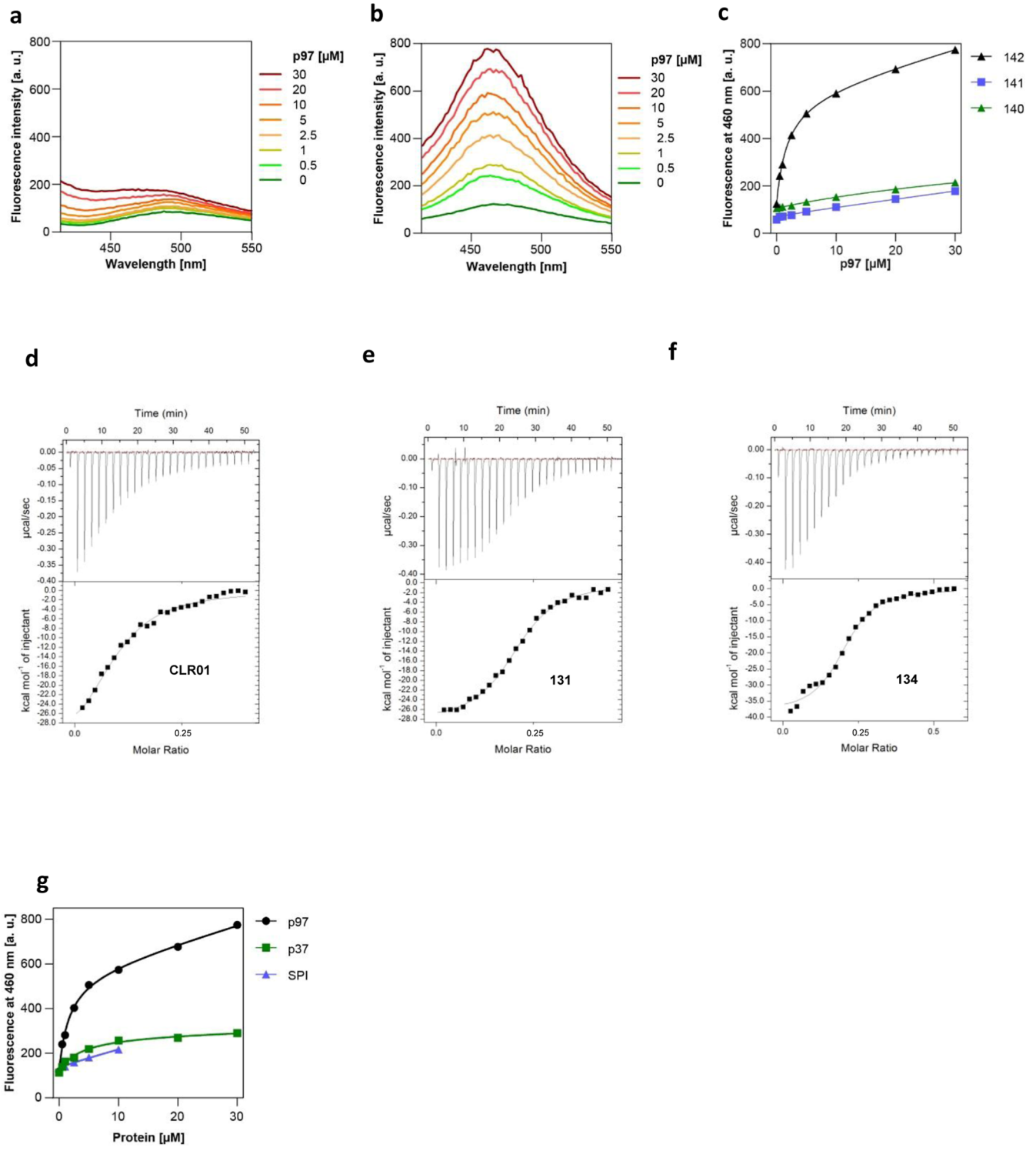


**Figure 3.** Affinity determination.

This amino acid host belongs to the class of molecular tweezers. It is constructed from alternating benzene and norbornadiene rings, which form an unpolar yet electron-rich cavity (Figure 1c,e). Only basic amino acids can enter this cavity with their cationic side chain, where they are bound by a powerful combination of Coulomb attraction and the hydrophobic effect (Figure 1d).[29] Lysine and Arginine recognition are fast and fully reversible events and do not interfere with natural protein function. Thus, molecular tweezers have already been used to develop inhibitors for specific protein protein interactions (Figure 1f).[30]

In a new approach, molecular tweezers were now coupled to various C3- and C6-symmetric core units, in order to provide candidates for a symmetric complexation of the accessible self-assembled D1 domain within the full-length protein p97. Such a binding event should sterically block the access of a misfolded protein to the central pore and prevent its unfolding and threading.



https://doi.org/10.1021/jacs.4c15288
J. Am. Chem. Soc. 2025, 147, 16836−16849

Protein symmetry has earlier been exploited by a few very elegant artificial protein ligands: The Bundle and Siegel groups constructed powerful toxin inhibitors from pentavalent arrangement of sugar units.[31,32] Hamilton and Trauner constructed tetravalent calixarenes for PDGF[33] and potassium channels,[34] which were later made photoswitchable.[35] However, this is the first blocking of a protein pore by a supramolecular ligand.

## RESULTS

In most of the above-described work/examples, the innovation came from chemical multiplication of a naturally occurring binding event. This differs greatly from the challenge of anchoring a multivalent amino acid binder over a protein pore: here we need sterically well accessible amino acid residues, which can be simultaneously complexed by each artificial binding unit. Although the cofactor machinery is recruited to the upper side of the D1 unit, where threading eventually takes place, molecular tweezers as potential pore plugs could in principle also bind to the D2 pore. To this end we closely inspected the D1 and D2 surface (PDB 5ftk) and identified several free-standing R and K residues which are not engaged in competing salt bridges.[23] Their distance from the central pore was used as a guide for the selection of the appropriate $C_3$- or $C_6$-symmetrical central core unit. The table in Figure 1h shows the average distance of selected accessible Lys and Arg residues ($\alpha$-C) from the respective pore center.[36] While the D1 pore features several basic residues within a distance of 20 Å, most arginines and lysines around the D2 pore are more than 20 Å away. Thus, a compact ligand design should favor the D1 pore. Our design concept is illustrated in Figure 1g–i: four selected well accessible lysines (pink/blue) are located in hexagonal arrangements around the central pore at varying distances (arrows in Figure 1g). A suitable pore (white) plug would now position three tweezer units (circles) in a triangular fashion over identical lysines close to the pore (here K-277) and prevent substrate access by sterically blocking the pore entrance with its symmetrical linker (Figure 1i).

Attachment of 3 or 6 terminal alkynes to a flat symmetrical scaffold in principle allows to conduct a three- or 6-fold Cu-catalyzed Click reaction with molecular tweezers carrying a terminal azide.[37] For such multiple 1,3-dipolar cycloadditions involving molecular tweezers, we have recently developed a very efficient synthetic protocol, which relies on iterative coupling in a one-pot reaction (Figure 2a).[38] This was now successfully applied to a large series of multivalent symmetrical tweezer oligomers, including those with the desired $C_3$- and $C_6$-symmetry (Figure 2b).

For comparison to the critical R and K distance the new multivalent tweezers were modeled in an extended conformation and the characteristic tweezer distances across their central hub were measured from the hydroquinone attachment point. The tweezer units in the whole series appear suited for simultaneous complexation of three up to six R or K residues at a distance of 10–20 Å from the D1 pore. Three prominent examples are given in Figure 2c. A survey of all multivalent tweezers and their tweezer distances is given in Figure S4. Various linkers place the tweezers at distances spanning between 20 and 40 Å, in principle suitable to reach most basic residues on the D1 surface.

The resulting new multivalent tweezer constructs were soluble in aqueous buffer and displayed no tendency for self-inclusion or aggregation (no aromatic upfield-shifts in the $^1$H NMR spectra, strong $M^+$ peaks in the HRMS spectra). They were examined in various biochemical and biophysical assays in order to characterize their affinity toward p97, their preferred binding epitope and their inhibitory potential of its protein unfolding machinery.

**Fluorescence Titrations.** It was anticipated that docking of the new multivalent tweezers with a central luminophore to the flat D1 surface would restrict internal rotations around the aromatic rings and thus turn-on fluorescence emission.[39−44] This was indeed the case and could be exploited to monitor binding to p97 and in some cases to determine affinities by conventional fluorescence titrations. A systematic series from mono- to hexavalent tweezers **140**–**145** containing binding sensitive luminophores, able to induce emission by a restriction of motion, was synthesized and their excitation as well as emission wavelengths were determined (Table S1). Excitation occurred at 360–430 nm, whereas emission wavelengths were in the range of 460–520 nm.

Constant tweezer concentrations (10 $\mu$M) were subsequently titrated with increasing p97 concentrations (0.5–30 $\mu$M); irradiation into the excitation maxima of all luminescent tweezers produced significant intensity changes, which were superior in the $C_3$- and $C_6$-symmetric binders indicating tight interaction with the protein surface.

Thus, trimer **142** led to an 8-fold increase in fluorescence intensity and nonlinear regression from the resulting binding isotherm gave a $K_d$ value of 1.8 $\mu$M (Figure 3b,c and Scheme S1b). By contrast, the related monomeric and dimeric tweezers **140** and **141** showed no binding to p97 (Figure 3a and Scheme S1a). While the tetrameric tweezer **143** produced almost no effect (Scheme S1c), trimeric and especially hexameric cyanostilbene tweezers **144** and **145** (Scheme S2a,b) bound strongly indicated by a more than 10-fold fluorescence increase. Multivalency of at least 3 appropriately placed tweezers seems to be a prerequisite for p97 recognition, and symmetry matters—only $C_3$ and $C_6$-symmetric tweezer derivatives are accepted.[45] This may be a first hint to preferential binding of basic residues around the pore of p97 by symmetrical multivalent tweezers. Unfortunately, several tweezers did not produce saturation curves so that their protein affinities could not be determined from fluorescence experiments (Scheme S3).

**ITC Experiments.** Multivalent tweezers without a built-in fluorophore were subjected to isothermal calorimetry (ITC) to determine affinity and thermodynamic parameters for the binding event (Figure 3d–f and Schemes S4–S6).[46] To this end, p97 was added stepwise to various tweezer solutions until saturation was reached. In all cases, tweezer binding to p97 was exothermic (Table 1). For the evaluation of all ITC binding curves, a "one set of sites" model was chosen for curve fitting, since all six binding sites are identical and no biphasic curves were obtained. Both nonfluorescent series (rigid vs flexible linkers) gave similar results to those found for the tweezers with built-in luminophores: Mono- and divalent tweezers again displayed very modest affinities to p97, while trimeric and higher oligomers bound tightly. The lowest $K_d$ values were determined for trivalent tweezer **131** ($K_d$ = 3.2 $\mu$M) and tetrameric **134** ($K_d$ = 2.5 $\mu$M). All these results are also in very good agreement with the unfolding assay (*vide infra*).

In an attempt to support K-277 and K-288 as primary targets of our multivalent tweezers, we exchanged both lysines by serines and performed ITC titrations between trimeric **142** and both mutants. This time, there was almost no enthalpic change


https://doi.org/10.1021/jacs.4c15288
J. Am. Chem. Soc. 2025, 147, 16836−16849

**Table 1. ITC Titrations of Oligomeric Tweezers with p97 and Thermodynamic Data**

| tweezer | $K_a$ [$M^{-1}$] | $K_d$ [$\mu$M] | $\Delta G$ kcal | $\Delta H$ kcal | $T\Delta S$ kcal | $n$ |
|---|---|---|---|---|---|---|
| **CLR01** monomer | 46,000 | 22 | −6.4 | −3.7 | −2.7 kcal | 10 |
| **131** flexible trimer | 314,000 | 3.2 | −7.5 | −6.0 | −1.5 kcal | 5 |
| **134** rigid tetramer | 400,000 | 2.5 | −7.6 | −7.9 | +0.3 kcal | 5 |
| **126** flexible dimer | n.d. | n.d. | n.d. | n.d. | n.d. | |
| **132** flexible tetramer | 44,000 | 23 | −6.3 | −5.7 | −0.6 kcal | 9 |
| **133** flexible pentamer | 29,000 | 35 | −6.2 | −12.2 | +6.0 kcal | 11 |
| **128** rigid dimer | n.d. | n.d. | n.d. | n.d. | n.d. | |
| **129** rigid trimer | n.d. | n.d. | n.d. | n.d. | n.d. | |
| **130** rigid trimer | 80,000 | 12 | −6.7 | −4.3 | −2.4 kcal | 13 |

and we could not obtain a binding curve from the titrations, so that the $K_d$ value must have increased considerably, at least to a value higher than 10−20 $\mu$M. This drastic change underlines the importance of K-277 and K-288 as anchor points of the trimeric tweezer **142** to the protein surface around the central pore (Scheme S6 D,E).

Contrary to **CLR01**, multivalent tweezers bind in a strongly enthalpy-driven mode. Unfavorable entropy terms may reflect the restricted rotation around many flexible bonds which takes place on multivalent docking of the large binders to the protein surface around the pore. Another factor may be incomplete desolvation of some lysines which cannot be fully included inside the tweezer cavity, weakening the hydrophobic effect.[47]

Unspecific binding of the tweezers to other factors in the unfolding reaction, rather than specifically to p97, could explain false positive effects in further functional assays. We therefore performed fluorescence binding experiments as above in which we compared binding to p97, to the p37 adapter or to the SDS22-PP1-I3 (SPI) substrate complex that are components of the unfolding assay described below. Importantly, the resulting binding curves demonstrate a high preference of the tweezer for p97, whereas no affinity could be determined for p37 and SDS22-PP1-I3 (Figure 3g).

**Protein Substrate Unfolding Assay.** To investigate the crucial protein threading event, we used a previously established assay (Figure 4a) that monitors protein unfolding associated with the processing of a PP1 complex by p97 during PP1 biogenesis.[15,48] In this process that can be reconstituted with purified proteins, PP1 catalytic subunit is bound by its partners "suppressor of-Dis2-number-2" (SDS22) and "inhibitor-3" (I3). Initially, the SDS22-PP1-I3 complex is recruited to p97 by the p37 substrate adapter. The insertion of I3 into the D1 pore and subsequent threading through the central channel leads to segregation of I3 (and SDS22) from PP1 and concomitant I3 unfolding. If I3 is fused experimentally to the fluorescent reporter protein mEos, I3 unfolding can be followed sensitively and in real time by the decay of mEos fluorescence. As expected, the competitive inhibitor CB-5083 strongly inhibited mEos-I3 unfolding (Figure 4b,c).[18] **CLR03** was used as negative control, because it resembles the tweezer, but lacks its sidewall and thus is unable to bind Lysine and Arginine; its Lewis structure is given in Figure 4 b.

Our analysis of the tweezer compounds demonstrated that 20 $\mu$M divalent luminescent tweezer **141** and both trivalent tweezers **131** as well as **142** strongly inhibit p97 activity, similar to 10 $\mu$M known inhibitor CB-5083 (Figure 4c). In contrast, **CLR01** acted only moderately and dimeric tweezer **126** was inactive. Hence, multivalent systems are superior to the monomeric parent tweezer.

With the most powerful inhibitor, trivalent luminescent tweezer **142**, unfolding was measured in a concentration-dependent fashion from 0.08 to 20 $\mu$M tweezer. Figure 4d reveals a steep ascent in unfolding activity from 1 to 2 $\mu$M tweezer and a corresponding $IC_{50}$ value of 1.1 $\mu$M, in line with its p97 affinity of 1.7 $\mu$M (Figure 4e).

Trimeric tweezer **142** was further characterized with respect to its influence on the formation of the unfolding machinery. Titration of the substrate adapter p37 to p97 and TAMRA-labeled SDS22-PP1-I3 gradually increased TAMRA fluorescence anisotropy up to an equimolar ratio of all components when saturation was reached indicating binding of SDS22-PP1-I3 to p97, as expected (Figure 4g). In contrast, in the presence of the tweezer **142**, fluorescence anisotropy was not further increased by addition of p37, even at a large excess of p37 demonstrating that trimeric tweezer **142** blocks the pore entrance and thus prevents formation of the unfolding machinery with the SPI substrate complex.

In order to facilitate structure activity relations, the functional unfolding assay was finally extended to all hitherto available multivalent tweezers (Figure 4f). In these measurements, the tweezer concentration was however lowered 10-fold from 20 to 2 $\mu$M, because the best trimeric tweezer **142** already binds with 2 $\mu$M affinity to p97. In the full synopsis of all multivalent tweezers, several other trimeric tweezers achieved a similar level as **142**, even more powerful effects were obtained with pentamer **133** and especially with hexamer **145**.

To identify the most probable tweezer binding sites (Figure 1g) we replaced selected single lysines (K-277 and K-288) in the immediate vicinity of the D1 pore by serines. Indeed, binding experiments with the trivalent luminescent tweezer **142** revealed a 6-fold and 11-fold higher $K_d$ for p97-K277S and p97-K288S, respectively, compared to wild type p97 (Scheme S7A−C)." Unfolding assays were performed with p97 full length proteins harboring either of the two mutations and were compared to wild type p97 (Figure 4h and Scheme S7D). Mutation of Lys-277 or Lys-288 to serine strongly impeded inhibition by tweezers **145** or **133** suggesting again that the two lysine residues are the prime interaction sites of the tweezer. Lys-277 and Lys-288 are located very close to the central pore at a distance of ∼20 and 26 Å, respectively. This binding site could be independently confirmed by MD simulations, which produced stable multivalent complexes with the best binders (especially with Trimer **142**) attached exclusively to Lys-277 sites (*vide infra*).[49]

These results demonstrate that symmetry and multivalency could be exploited in a favorable way and furnished efficient new inhibitors for the central protein pore.

**ATPase Assay.** Although different nucleotide states of p97 can adopt a planar configuration in the absence of substrate,[23] the full ATPase activity of p97 likely involves the sequential movement of the subunits of the p97 hexamer similar to the movements during substrate unfolding.[25,26] We therefore expected that, conversely, constraining subunit movement by tweezer binding should lead to a reduction of ATPase activity. We performed ATPase assays that are coupled to concomitant dephosphorylation of phosphoenolpyruvate to pyruvate by


https://doi.org/10.1021/jacs.4c15288
J. Am. Chem. Soc. 2025, 147, 16836−16849

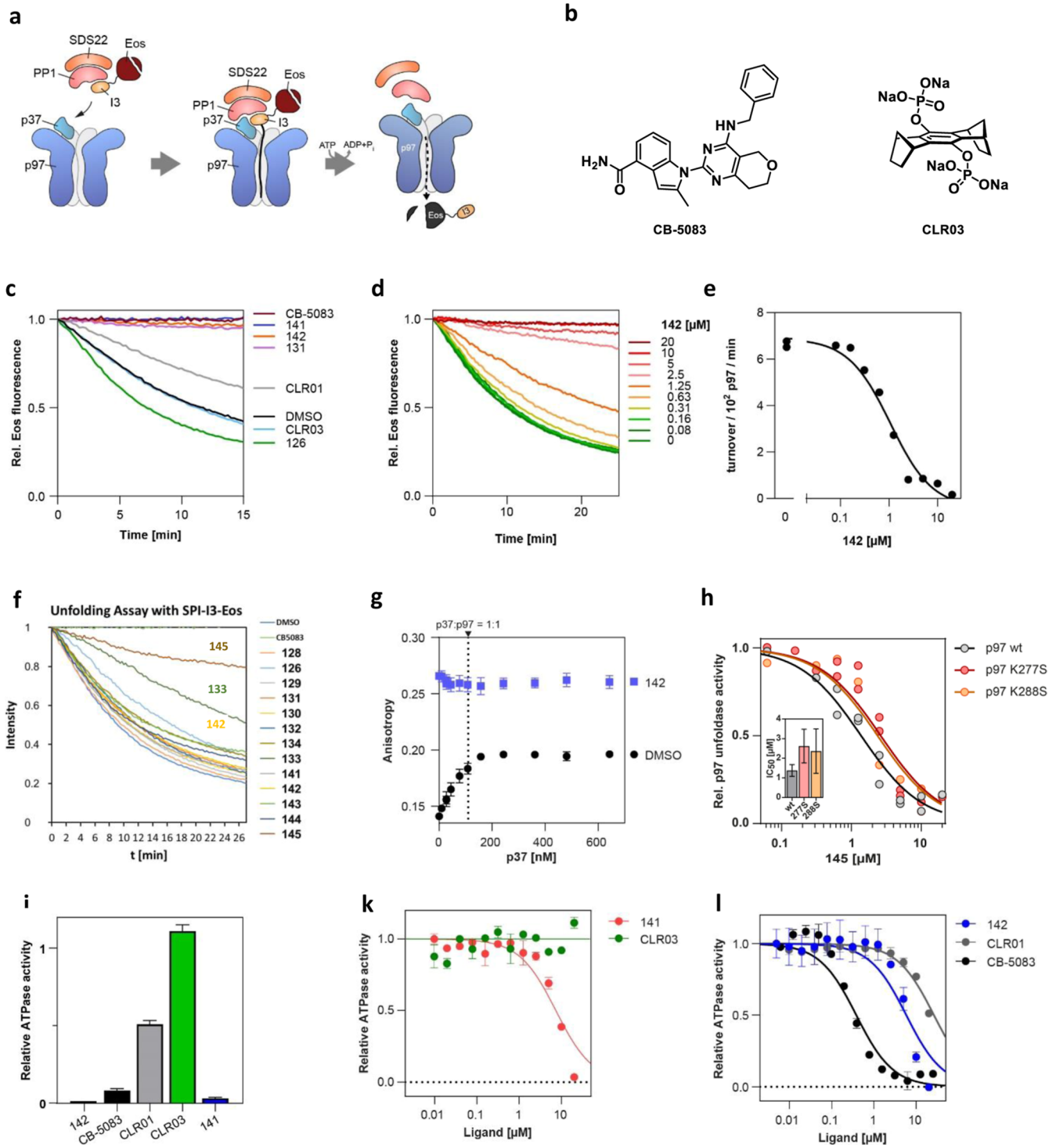


**Figure 4.** Unfolding and ATPase assay.

pyruvate kinase, which is in turn reduced to lactate by lactate dehydrogenase and consumes the cofactor NADH (Figure 4i). In such an ATPase experiment, decreasing NADH absorption at 340 nm over time thus indicates ATPase activity.[50] In the presence of 10 $\mu$M luminescent tweezers **141** and **142** as well as the competitive inhibitor **CB-5083**, the ATPase activity of p97 was indeed strongly inhibited (Figure 4k). **CLR01** only displayed a moderate effect while the negative control **CLR03** did not lead to significant change. In a concentration-dependent experiment, the efficiency of both multivalent tweezers over **CLR01** and **CLR03** is illustrated by a significant shift of the activity curves toward lower concentrations (Figure 4l,m). This experiment corroborates a significant influence of multivalent tweezer binding on ATPase activity of the p97 segregase.

**Structural Biology.** Several pieces of experimental evidence have now been provided for supramolecular pore blocking by our multivalent tweezers. For a final proof we sought independent support from structural biology. However, all crystallization attempts of the 1:1 complex between p97 and



https://doi.org/10.1021/jacs.4c15288
J. Am. Chem. Soc. 2025, 147, 16836−16849

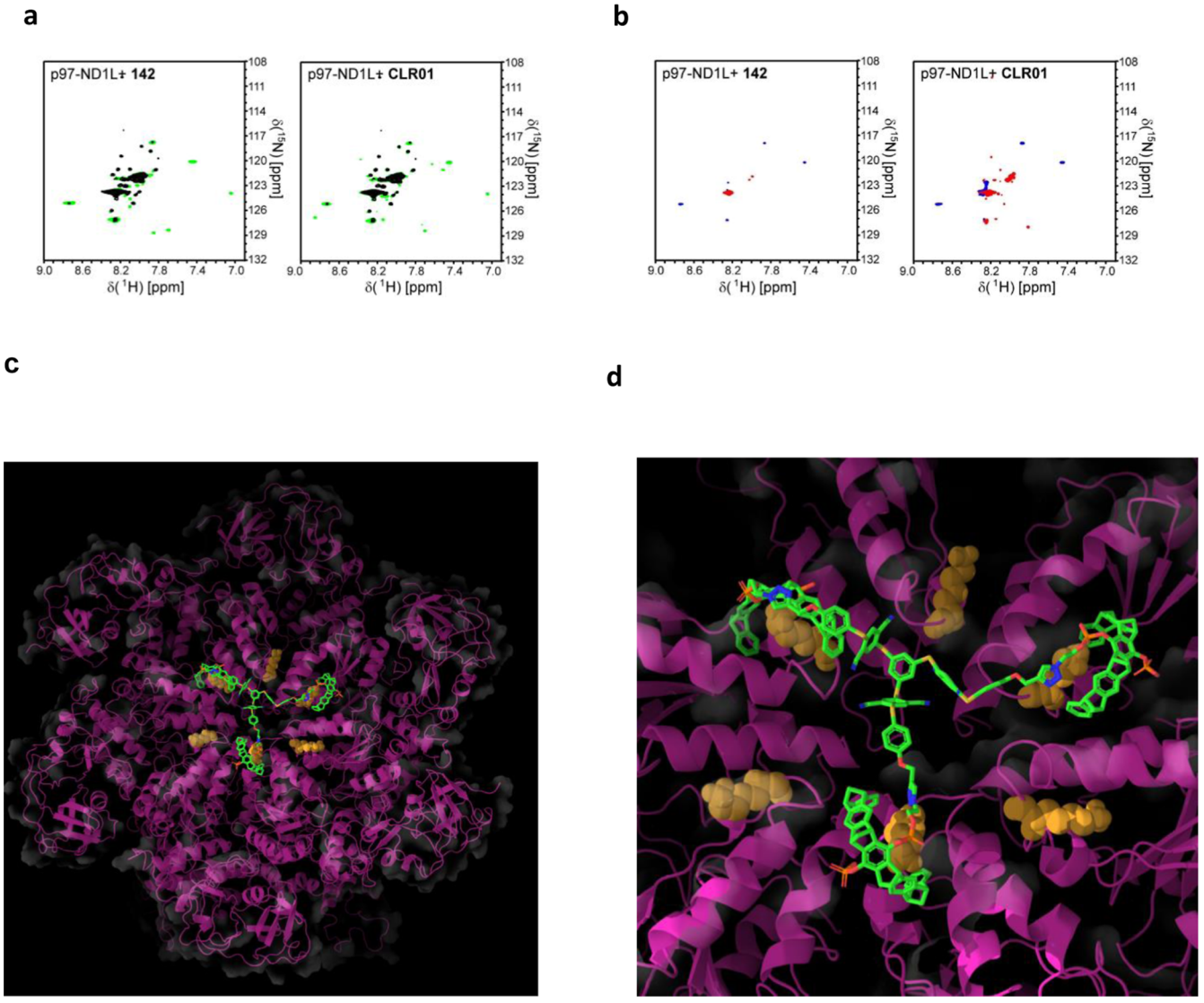


**Figure 5.** Structural biology and computational modeling.

trimeric tweezers were futile.[51] Likewise, assignment of the most probable tweezer binding sites by NMR spectroscopy could not be accomplished, because the four lysine-to-serine mutants which were already used in the unfolding assay, produced ambiguous results in the $^{15}$N-BEST-TROSY-HSQC spectrum (Figure 5a).[52] Nevertheless, $^{15}$N-HSQC titrations of the lysine-labeled ND1 domain with **CLR01** and trimer **142** reveals qualitative differences between the two tweezers (Figure 5b): **CLR01** produced more new peaks (both positive and negative) in the difference spectrum while the trimer, which was optimized for **K-277**, showed less differences, indicating higher specificity (Figures S2 and S3).

**Computational Modeling.** In order to visualize a potential multivalent tweezer binding to the identified Lysine residue K-277 in the immediate vicinity of the D1-pore MD simulations were performed with explicit solvent treatment in aqueous buffer at pH 7.[53,54] Tweezers **142**, **133** and **145** were placed above the central pore and subjected to 100 ns calculation at 25 °C. After this time, trimer (Figure 5c,d) and hexamer (Figure S1) were still found firmly bound in a multivalent fashion to the ring of K-277 indicating that this represents a favorable binding mode. By contrast, pentamer **133** turned out to be too small to reach all K-277 lysines and bound in an unsymmetric fashion to a few residues K-277 and K-323. Careful analysis of the preferred binding mode reveals a close correlation between the size of the core unit and the pore distance of the respective lysine target: only if all tweezers can reach their lysine counterparts highly efficient multivalent binding and pore blocking will be established. It should be noted that the highest lysine density is found near the central pore; therefore small compact core units with a large number of tweezers will outcompete extended scaffolds because multivalent docking becomes much more challenging when lysines are standing far away from each other.

## DISCUSSION

In the course of this project, a large number of different multivalent tweezer molecules was synthesized. For the first time a hexameric tweezer could be prepared by the new iterative click procedure, demonstrating its high efficiency. Rigid core structures may pose solubility problems approaching higher oligomers, so that the solvent system must be adjusted accordingly; however the click reaction tolerates a wide variety of solvents of different polarity.[55]



https://doi.org/10.1021/jacs.4c15288
J. Am. Chem. Soc. 2025, 147, 16836−16849

In Figure 2 the new multivalent tweezer structures are grouped into 3 classes: (a) **128**−**134** contain rigid aromatic spacers, **126**−**133** rely on flexible esters, whereas **140**−**145** carry a central binding sensitive luminophore unit based on aromatic thioethers and cyanostilbenes. It appears that symmetry and multivalency matter—notably in all assays the best results were obtained with $C_3$- and $C_6$-symmetric tweezer ligands. Both rigid and flexible spacers lead to powerful binders and unfolding inhibitors of p97, so that preorganization is most likely not a prerequisite for multivalent recognition, possibly because after docking of the first tweezer on a favorable lysine residue, the other (quasi-intramolecular) contacts are made much more easily due to the lowered overall complex entropy. Thus, the repertoire of suitable $C_3$- and $C_6$-symmetric core units is large and may be adjusted to the specific amino acid distances from each other and the pore.[56]

We would like to emphasize that the luminophore sensor groups turned out to be highly advantageous, because their induced emission indicated directly when strong binding occurred and could in some cases even be utilized for a quantitative affinity determination from fluorescence titration. Hence the full series from dimeric to hexameric luminescent tweezer **140**−**145** constitutes the first example of protein-selective luminophors with a high preference for flat protein flanks. Restricted rotation around the chromophore bonds is efficiently realized by the symmetrical attachment of all tweezer moieties on their respective basic amino acid counterparts on the protein surface. At this moment we cannot explain why the significant induced emission intensity does not produce a binding curve for all representatives of this new binding sensitive luminescent tweezer family.

Generally, even the hexameric tweezers become water-soluble after neutralization of their phosphoric acid precursors. In some cases, however, a small DMSO content (2−3%) was necessary to ensure complete solubility throughout the entire biological experiment. NMR spectra are concentration-independent and produce sharp signals, without appearance of substantial upfield shifts indicative of self-inclusion inside their multiple cavities.

For an efficient blocking of the pore entry a core unit with extended aromatic rests would be advantageous for the multivalent tweezer design. This must certainly be balanced with a potential insolubility of the growing solvent-exposed aromatic area. For very large proteins we envisage to employ prototypic core structures of high shape fidelity such as Höger's giant macrocycles, since such constructs would be able to cover an entire protein flank.[57]

Binding efficiency steadily increases with the number of tweezer units, however/albeit not linearly: there seems to be some degree of negative cooperativity, most likely because 6 simultaneous tweezer lysine contacts require a perfect complementarity on a flat hexagon.[58] ITC measurements of flexible and rigid tweezer oligomers produce affinities in the low micromolar range comparable to those of the binding sensitive luminophores. Apart from the fact that all new tweezer oligomers bind to p97 in an enthalpy-driven sense, enthalpic and entropy changes quite often counterbalance each other—a phenomenon known as entropy enthalpy compensation.[47] In Table 1 the contributions of both factors are listed and shed more light on the binding mechanism: unfavorable entropy terms are mainly produced by large binders, possibly originating from restricted rotation on multivalent docking and/or from incomplete desolvation of weakly bound lysines.

Taken together, experimental evidence was accumulated for the specific blocking of the central p97 pore: strong hindrance of protein unfolding, concomitant with inhibition of ATPase activity and formation of the unfolding-machinery all point to competitive binding of multivalent tweezers to the pore entrance.

Without detailed information from structural biology, it is difficult to estimate the selectivity of the most powerful unfolding inhibitors for the symmetrical environment around the pore versus other lysine-rich areas on the very large self-assembled protein. However, the significant improvement of unfolding inhibition in tweezers with the right symmetry clearly speaks for a strong preference of C3 and C6-symmetrical tweezers for the immediate vicinity of the central pore with a maximum number of potential tweezer lysine contacts. Specific binding close to the pore entry was further validated with the K-277 mutant in the unfolding assay and supported by MD simulations.

## CONCLUSION

This work introduces the first supramolecular element designed to cover the pore of a protein machine. Imitating the natural symmetry of AAA+ ATPases, multivalent molecular tweezers have been synthesized which explore the regular arrangement of lysines and arginines around the functional protein pore of the essential and medically relevant segregase p97 (Scheme S5). Some of these ligands carry a core unit capable of binding sensitive emission as convenient readout for protein recognition.

Docking of the tweezer units onto their anchor points around the central pore of p97 is accompanied by a strong fluorescence signal and simultaneously inhibits unfolding and threading of the protein substrate through the pore of the protein machine. This effect was studied with various biophysical methods and state-of-the-art biochemical activity assays, as well as validated independently by mutagenesis.

The new pore plugs represent a novel class of synthetic receptor molecules that may serve to study aspects of the molecular mechanism of p97 or related proteins, e.g. with respect to the highly dynamic internal protein motion, its coupling with ATP hydrolysis or substrate entry through one or both pore entries.

Tweezer constructs with the correct symmetry and optimized multivalency may also be used to study and influence other protein pores. In this respect they may become a valuable class of supramolecular chemical tools to elucidate the mechanism of various dynamic pores and to prepare potent inhibitors for their mechanism of action.

Since p97 and related protein machines are vital to protein quality control and cell survival, specific inhibitors may be used to combat diseases. Our contribution will therefore help supramolecular chemists and protein biologists to address well-defined protein pores by rational design, with implications for drug discovery.

## EXPERIMENTAL SECTION

**General Procedure for the Iterative Click Reaction between Polyvalent Alkynes and the Azidotweezer to Prepare Multivalent Tweezers.** Under argon atmosphere monophosphate monoethylazidophosphate tweezer **1** (10.0 mg, 0.01 mmol, 1.0 equiv) and alkyne (1.0 equiv) were dissolved in dry THF (2 mL), $H_2O$ (1 mL) and DIPEA (8.77 mg, 11.9 μL, 0.07 mmol, 5.4 equiv). The transparent solution was stirred for 5 min at room temperature. A



https://doi.org/10.1021/jacs.4c15288
J. Am. Chem. Soc. 2025, 147, 16836−16849

solution of copper sulfate pentahydrate (8.30 mg, 0.03 mmol, 3 equiv) and sodium ascorbate (13.0 mg, 0.07 mmol, 5.2 equiv) in $H_2O$ (1 mL) was added to the reaction mixture and stirred for 16 h. Reaction control was performed via HPLC analysis of small samples taken directly from the reaction mixture. After complete consumption of the starting material, another equivalent of azidotweezer **1** was added in situ (10.0 mg, 0.01 mmol, 1.0 equiv). Likewise, the whole reagent cocktail, i.e., DIPEA (8.77 mg, 11.9 μL, 0.07 mmol, 5.4 equiv), dry THF (1 mL), copper sulfate pentahydrate (8.30 mg, 0.03 mmol, 3 equiv) and sodium ascorbate (13.0 mg, 0.07 mmol, 5.2 equiv) dissolved in water (1 mL), was again added in situ. This sequence was repeated as often as tweezer units could be accommodated in the final product. After full conversion was reached via HPLC control, the solvent was removed under vacuum and HCl (aq., 1 M, 30 mL) was added. The suspension was transferred into a falcon tube and sonicated twice for 15 min. After centrifugation for 15 min at 4000 rpm, the solvent was decanted, and the solid residue was isolated. It was washed with $H_2O$ (30 mL) and with $Et_2O$ (30 mL). After isolation via centrifugation, the multivalent tweezer was dissolved in mixture of THF and $H_2O$ (1:1). After lyophilization, the desired product was obtained as the free phosphoric acid.

The multivalent diphosphoric acid tweezer derivative was obtained as a colorless solid in moderate to good yield. Conversion to the sodium salt was performed by dissolving the free diphosphoric acid (1.0 equiv) in a 1:1 mixture of MeCN/$H_2O$ (5 mL). Aq. NaOH (0.23 M, 1.0 eq. for each tweezer unit) was added, and the reaction mixture was stirred for 1 h at room temperature. The solvent was removed under vacuum and the compound was lyophilized. The sodium salt product was obtained as a colorless solid in quantitative yield.

**Fluorescence Titrations (140−145 on p97, p37 and SPI).** Fluorescence titrations were performed on a Cary Eclipse fluorescence spectrometer (Varian). Stock solutions were prepared in 25 mM HEPES buffer (pH 7.5, 100 mM KCl, 5 mM $MgCl_2$, 1 mM DTT) for tweezers and protein containing 500 μM tweezer and 73.5 μM p97. These were combined and diluted with buffer to 60 μL in 1.5 mL Eppendorff tubes, resulting in a constant concentration of 10 μM tweezers and increasing concentrations of p97 (0, 0.5, 1.0, 2.5, 5.0, 10, 20, 30 μM). After thorough mixing fluorescence spectra were recorded at 25 °C for each sample. Tweezers **140−143** were excited at 360 nm, tweezers **144** and **145** at 430 nm. Emission was recorded between 400 and 600 nm.

The increase in fluorescence intensity at the emission maximum relative to protein concentrations produced binding curves which were subjected to nonlinear regression and furnished $K_d$ values in the low micromolar range. Fits were performed in GraphPad Prism 10 using the standard equation for binding corrected for nonspecific background binding; $Y = B_{max} \times X/(K_d + X) + NS \times X + Background$, where $B_{max}$ is the signal at maximum binding, NS is the slope of nonspecific binding and Background is the starting fluorescence of the tweezer without additional protein.

IC50 Curves were fit using the standard IC50 equation $Y = Bottom + (Top - Bottom)/(1 + (X/IC_{50}))$ with Top and Bottom as activity at minimum and maximum inhibition (i.e., 1 and 0).

**Isothermal Titration Calorimetry (ITC) Titrations (CLR01, 126, 131).** ITC titrations were conducted on a MicroCal iTC200 (Malvern Panalytical) operated at 25 °C with a reference power of 5 μcal/s. The respective molecular tweezer (10−100 μM) dissolved in PBS buffer (pH 7.4, 25 °C) was provided in the cell and titrated with 100 μM purified p97 in the titration syringe (reverse titration). After an initial 0.4 μL injection, 18 consecutive 2.0 μL injections at time intervals of 180 s were performed. Run data were processed using the instrument software Origin (v7.0552), and binding isotherms were fitted to the "one set of sites" model. Stoichiometry values $n(1,1)$ were obtained from refinement with the AFFINImeter software (Cloud version v2.1802.5) using the independent one site fitting approach (see Supporting Information). From the enthalpy measurement ($\Delta H$) and the determined free complexation enthalpy $\Delta G$, entropy changes $\Delta S$ were calculated; these are shown in the Supporting Information.

**Protein Expression and Purification.** Recombinant GST-p37, p97 and variants thereof were expressed in *Escherichia coli* BL21 (DE3) and purified as previously described (PMID 12847084, PMID 33058883). In brief, GST-p37 was isolated using GSTrap (Cytiva), GST was removed by PreScission protease and p37 was purified on a Superdex 75 16/600 in p97 buffer (50 mM HEPES pH 7.5, 150 mM KCl, 1 mM, $MgCl_2$, 5% glycerol, 1 mM DTT). His-tagged p97 was purified using HisTrap (Cytiva) followed by anion exchange using Q-HP (Cytiva) and buffer exchange to p97 buffer. SDS22, PP1γ and His-Inhibitor-3-mEos3.2 (SPIE) were copurified as a complex from High Five insect cells as previously described.[59] In brief, SPIE was isolated using HisTrap, followed by Q-HP anion exchange and gel filtration on a Superdex 200 16/600 column (Cytiva) in p97 buffer. For generation of SPI-TAMRA, SPI with C-terminal sortase tag in Inhibitor-3 was purified as described for SPIE. Subsequently, a GGGWSHPQFEK- TAMRA peptide (Caslo APS) was conjugated to the sortase tag in Inhibitor-3 via sortase-mediated ligation, as previously described[48] and the labeled protein was isolated via StrepTrap (Cytiva) and gel filtration on a Superdex 200 16/600 column.

A backbone break was introduced into mEos 3.2 by irradiation with a Blak-Ray UV lamp (B-100AP) for 2 h on ice. Proteins were concentrated, snap-frozen and stored at −80 °C.

**Fluorescence Anisotropy.** p37-dependent binding of SPI-TAMRA (100 nM) to p97 (100 nM) in assay buffer was followed via fluorescence anisotropy. For this, fluorescence anisotropy of TAMRA was followed in a Varian Cary Eclipse spectrofluorometer (excitation wavelength, 520 nm; emission wavelength, 580 nm; excitation slit, 20 nm; emission slit, 20 nm; temperature, 25 °C) upon addition of p37.

**Fluorescence-Based Binding and Activity Assays.** p97-mediated unfolding activity was determined via loss of Eos fluorescence during unfolding of Inhibitor-3-Eos, as previously described (PMID 33058883). In brief, p97 (85 nM), p37 (150 nM) and SPIE (85 nM) were mixed in assay buffer (25 mM HEPES pH 7.4, 100 mM KCl, 5 mM $MgCl_2$, 1 mM DTT) and baseline fluorescence was recorded for at least 3 min at 25 °C before ATP was added to a final concentration of 2 mM and the fluorescence emission at 580 nm was measured every 15 s over 40 min (excitation wavelength, 540 nm; excitation slit, 10 nm; emission slit, 10 nm; temperature, 25 °C).

Fluorescence spectra of luminescent tweezers (1 μM) were recorded in a Varian Cary Eclipse spectrofluorometer (Varian) upon excitation at 360 nm (excitation slit, 20 nm; emission slit, 20 nm; temperature, 20 °C). Data was fitted in GraphPad Prism 10.0.2 to the standard single-site binding model corrected for nonspecific background binding: $Y = B_{max} \times X/(K_d + X) + NS \times X + Background$, where $B_{max}$ is the signal at maximum binding, NS is the slope of nonspecific binding and Background is the starting fluorescence of the tweezer without additional protein.

**ATPase Assay.** His-p97 (250 nM) was incubated with LDH/PK enzyme mix (~3.8/~5.6 units; Sigma), PEP (7.5 mM) and NADH (0.6 mM) in assay buffer with indicated tweezer concentrations. The reaction was started by addition of ATP (2 mM) and the absorbance at 340 nm was followed for 30 min at 37 °C in a SpectraMax Plus 384 (Molecular Devices) spectrophotometer. Activity was calculated from the slopes during linear absorbance decrease. Experiments were performed in technical duplicates and data was fitted in GraphPad Prism 10.0.2 for $IC_{50}$ using the standard equation $Y = Bottom + (Top - Bottom)/(1 + (X/IC_{50}))$ with Top and Bottom as activity at minimum and maximum inhibition (i.e., 1 and 0).

**NMR Spectroscopic Experiments: HSQC CLR01/p97 and 142/p97. Expression and Purification of $^2H$, $^{15}N$-Lys-p97-ND1L.** $^2H$,$^{15}N$-Lys isotope-labeled p97-ND1L (1−480) with an N-terminal $His_6$-tag was cloned into a modified pET15b vector using NdeI/*Bam*HI restriction sites.

$^2H$,$^{15}N$-Lys-p97-ND1L (wt and mutants) was expressed in *E. coli* Rosetta2 in Minimal Media with unlabeled $NH_4Cl$, 99% $D_2O$ and $^{15}N$-Lysine (1 g/L). The addition of $^{15}N$-Lysine in the presence of unlabeled $^{14}NH_4Cl$ results in $^{15}N$-labeling of only those amide NHs that belong to lysine, thus only lysine NH are visible in the $^{15}N$-HSQC spectrum.



https://doi.org/10.1021/jacs.4c15288
J. Am. Chem. Soc. 2025, 147, 16836−16849

Protein expression was induced with 1 mM IPTG overnight at18 °C. The protein was purified by Ni-affinity chromatography in PBS buffer (pH 7.5) and subsequently concentrated and buffer-exchanged into NMR buffer (25 mM HEPES pH 7.5, 50 mM NaCl, 5 mM TCEP) using centrifugal concentrators (10 kDa MWCO, Vivaspin).

Point mutants (K277S, K288S, L336S, K386S) were generated using the Quikchange Site-directed Mutagenesis Protocol (Agilent) and expressed and purified with $^{2}H$,$^{15}N$-Lys labeling as described for the wild type (wt).

**Protein NMR Spectroscopy.** Protein NMR experiments were performed on a Bruker 700 MHz Avance NMR spectrometer (Bruker, Germany) with a 5 mm TCI cryoprobe with z-gradient at 25 °C. The $^{1}H-^{15}N$-BEST-TROSY-HSQC pulse program is part of the NMRlib 2.0 pulse sequence tools library from IBS (Grenoble, France, https://www.ibs.fr/en/communication-outreach/scientific-output/software/nmrlib-2-0-ibs-pulse-sequence-tools-for-bruker-spectrometers/).[52] Spectra were processed and subtracted with Topspin 3.5 (Bruker) and visualized in CARA.[60]

Protein NMR samples contained $^{2}H$, $^{15}N$-Lys-p97-ND1L (400 $\mu$M, 200 $\mu$L) in NMR buffer (25 mM HEPES pH 7.5, 50 mM NaCl, 5 mM TCEP) with 10% $D_2O$ in 3 mm sample tubes. $^{1}H-^{15}N$-BEST-TROSY-HSQC NMR spectra (256 increments, 896 scans, experiment time 24 h) of wt, mutants and controls (see below) were recorded at 25 °C. Since only lysines carry the $^{15}N$ label, only these residues are visible in the spectrum.

Compared to the wt, mutants in which one lysine has been replaced by serine are expected to lack one specific signal, which allows to assign this mutated lysine. In a mutant−wt difference spectrum, this should result in one single negative peak. Unfortunately, more changes between mutant and wt spectra were observed, likely due to a change in protein dynamics, and thus the lysine residues could not be assigned.

For the NMR titrations with tweezers, a 7 mM stock solution of **CLR01** or **142** in water with 3% DMSO-$d_6$ was added stepwise (0, 50, 100, 200, 400 $\mu$M) to $^{2}H$, $^{15}N$-Lys-p97-ND1L (400 $\mu$M) up to a 1:1 ratio. $^{1}H-^{15}N$-BEST-TROSY-HSQC NMR spectra were recorded for each titration step. In addition, control spectra of $^{15}N$-Lys-p97-ND1L (400 $\mu$M) with the maximum amount of DMSO-$d_6$ (0.17% v/v, without tweezers) and protein incubated at 25 °C without ligand for the total duration of the titration experiment (5 d) were recorded. For the difference spectra, the control spectrum without tweezers (5 d at 25 °C) was subtracted from the spectrum with 1 equiv (400 $\mu$M) Tweezers. The control samples before and after incubation at 25 °C for 5 d and mutant proteins were analyzed on an SDS-PAGE gel to ensure that no visible degradation occurred over the time period of the NMR experiment and that mutants show a comparable degree of purity.

**Computational Modeling p97-ND1.** The protein coordinates were retrieved from the PDB entry 5FTK.[23] This structure was used in the protein preparation wizard of the Maestro program,[61] including addition of missing hydrogen and side chain atoms. The protonation states were assigned using PROPKA at pH 7.4. A restrained minimization (OPLS_2005 force field) was used to relax the protein prior to any further steps.[54]

The lysine residue Lys277 at the D1 Pore was selected for tweezer placement. Three identical lysines (every second) were selected for the trivalent tweezer ABS142 and six identical lysines were used to dock the hexavalent tweezer ABS145.

Molecular dynamics (MD) simulations were performed with the Desmond program.[62] The protein was placed in an orthorhombic box (at least 10 Å from the protein to the walls of the box in all directions) and solvated with SPC water. The charges were neutralized by the addition of sodium ions, and sodium chloride was added to a total concentration of 150 mM. The MD simulation was set up to run for 200 ns in total for the full protein. The trajectory was saved, resulting in 2084 trajectory frames (energy saved every 1.2 ps). The simulations were run in the *NPT* ensemble at 300 K and 1013 mbar. The model system was relaxed before the production run by the standard relaxation protocol provided.

For analysis and visualization, the MD simulation was subjected to cluster analysis, which revealed the most abundant structures of the simulation. These structures were analyzed regarding their binding mode. Visualization was achieved with the Pymol program. For the schematic representation, distances of the selected lysines and arginines were also measured in Pymol.

## ■ ASSOCIATED CONTENT

### Supporting Information

The Supporting Information is available free of charge at https://pubs.acs.org/doi/10.1021/jacs.4c15288.

Synthetic procedures, NMR and MS characterization, MD simulation, excitation and emission maxima, fluorescence titrations, binding curves, ITC titrations, stability tests, HSQC spectra (PDF)

## ■ AUTHOR INFORMATION


### Corresponding Authors

**Hemmo Meyer** − *Faculty of Biology, University of Duisburg-Essen, 45141 Essen, Germany*; Email: hemmo.meyer@uni-due.de

**Thomas Schrader** − *Faculty of Chemistry, University of Duisburg-Essen, 45141 Essen, Germany*; orcid.org/0000-0002-7003-6362; Email: thomas.schrader@uni-due.de

### Authors

**Abbna Kirupakaran** − *Faculty of Chemistry, University of Duisburg-Essen, 45141 Essen, Germany*; orcid.org/0000-0002-3954-9936

**Johannes van den Boom** − *Faculty of Biology, University of Duisburg-Essen, 45141 Essen, Germany*

**Mike Blueggel** − *Faculty of Biology, University of Duisburg-Essen, 45141 Essen, Germany*; orcid.org/0000-0002-8963-256X

**Christine Beuck** − *Faculty of Biology, University of Duisburg-Essen, 45141 Essen, Germany*; orcid.org/0000-0001-7513-7384

**Felix Niemeyer** − *Faculty of Chemistry, University of Duisburg-Essen, 45141 Essen, Germany*; orcid.org/0000-0002-9145-773X

**Matthias Hayduk** − *Faculty of Chemistry, University of Duisburg-Essen, 45141 Essen, Germany*

**Jan Balszuweit** − *Faculty of Chemistry, University of Duisburg-Essen, 45141 Essen, Germany*

**Peter Bayer** − *Faculty of Biology, University of Duisburg-Essen, 45141 Essen, Germany*; orcid.org/0000-0003-0435-7202

**Jens Voskuhl** − *Faculty of Chemistry, University of Duisburg-Essen, 45141 Essen, Germany*

Complete contact information is available at: https://pubs.acs.org/10.1021/jacs.4c15288

### Author Contributions

[§]A.K. and J.v.d.B. contributed equally to this work.



### Funding

T.S., H.M., P.B. and J.V. received funding from the German Research Foundation (DFG) in the context of the Collaborative Research center CRC1093 "Supramolecular Chemistry on Proteins".


### Notes

The authors declare no competing financial interest.

## ■ ACKNOWLEDGMENTS

T.S., H.M., P.B. and J.V. gratefully acknowledge generous financial support from the German Research Foundation (DFG) as principal investigators in the Collaborative Research centre CRC1093 "Supramolecular Chemistry on Proteins".

## ■ REFERENCES

(1) Woolley, G. A. Photocontrolling peptide alpha helices. *Acc. Chem. Res.* **2005**, *38*, 486−493.
(2) Nowick, J. S. Exploring β-Sheet Structure and Interactions with Chemical Model Systems. *Acc. Chem. Res.* **2008**, *41* (10), 1319−1330.
(3) Horne, W. S.; Johnson, L. M.; Ketas, T. J.; Klasse, P. J.; Lu, M.; Moore, J. P.; Gellman, S. H. Structural and biological mimicry of protein surface recognition by α/β-peptide foldamers. *Proc. Natl. Acad. Sci. U.S.A.* **2009**, *106*, 14751−14756.
(4) Chinai, J. M.; Taylor, A. B.; Ryno, L. M.; Hargreaves, N. D.; Morris, C. A.; Hart, P. J.; Urbach, A. R. Molecular recognition of insulin by a synthetic receptor. *J. Am. Chem. Soc.* **2011**, *133*, 8810−8813.
(5) Fletcher, S.; Hamilton, A. D. Protein surface recognition and proteomimetics: mimics of protein surface structure and function. *Curr. Opin. Chem. Biol.* **2005**, *9*, 632−638.
(6) O'Brien, J.; Shea, K. J. Tuning the Protein Corona of Hydrogel Nanoparticles: The Synthesis of Abiotic Protein and Peptide Affinity Reagents. *Acc. Chem. Res.* **2016**, *49*, 1200−1210.
(7) Klein, A. N.; Ziehm, T.; van Groen, T.; Kadish, I.; Elfgen, A.; Tusche, M.; Thomaier, M.; Reiss, K.; Brener, O.; Gremer, L.; Kutzsche, J.; Willbold, D. Optimization of D-Peptides for Aβ Monomer Binding Specificity Enhances Their Potential to Eliminate Toxic Aβ Oligomers. *ACS Chem. Neurosci.* **2017**, *8*, 1889−1900.
(8) Dang, D. T. Molecular Approaches to Protein Dimerization: Opportunities for Supramolecular Chemistry. *Front. Chem.* **2022**, *10*, 829312.
(9) Stevers, L. M.; Sijbesma, E.; Botta, M.; MacKintosh, C.; Obsil, T.; Landrieu, I.; Cau, Y.; Wilson, A. J.; Karawajczyk, A.; Eickhoff, J.; Davis, J.; Hann, M.; O'Mahony, G.; Doveston, R. G.; Brunsveld, L.; Ottmann, C. Modulators of 14−3-3 Protein-Protein Interactions. *J. Med. Chem.* **2018**, *61*, 3755−3778.
(10) Merdanovic, M.; Burston, S. G.; Schmitz, A. L.; Köcher, S.; Knapp, S.; Clausen, T.; Kaiser, M.; Huber, R.; Ehrmann, M. Activation by substoichiometric inhibition. *Proc. Natl. Acad. Sci. U.S.A.* **2020**, *117*, 1414−1418.
(11) Jiang, Q. Q.; Sicking, W.; Ehlers, M.; Schmuck, C. Discovery of potent inhibitors of human β-tryptase from pre-equilibrated dynamic combinatorial libraries. *Chem. Sci.* **2015**, *6*, 1792−1800.
(12) Snider, J.; Thibault, G.; Houry, W. A. The AAA+ superfamily of functionally diverse proteins. *Genome Biol.* **2008**, *9*, 216.
(13) Meyer, H.; Weihl, C. C. The VCP/p97 system at a glance: connecting cellular function to disease pathogenesis. *J. Cell Sci.* **2014**, *127*, 3877−3883.
(14) van den Boom, J.; Meyer, H. VCP/p97-Mediated Unfolding as a Principle in Protein Homeostasis and Signaling. *Mol. Cell* **2018**, *69*, 182−194.
(15) Weith, M.; Seiler, J.; van den Boom, J.; Kracht, M.; Hülsmann, J.; Primorac, I.; Del Pino Garcia, J.; Kaschani, F.; Kaiser, M.; Musacchio, A.; Bollen, M.; Meyer, H. Ubiquitin-Independent Disassembly by a p97 AAA-ATPase Complex Drives PP1 Holoenzyme Formation. *Mol. Cell* **2018**, *72*, 766−777.
(16) Buchberger, A.; et al. Control of p97 function by cofactor binding. *FEBS Lett.* **2015**, *589*, 2578−2589.
(17) Meyer, H.; van den Boom, J. Targeting of client proteins to the VCP/p97/Cdc48 unfolding machine. *Front. Mol. Biosci.* **2023**, *10*, 1142989.
(18) Anderson, D. J.; et al. Targeting the AAA ATPase p97 as an Approach to Treat Cancer through Disruption of Protein Homeostasis. *Cancer Cell* **2015**, *28*, 653−665.
(19) Huryn, D. M.; et al. p97: An Emerging Target for Cancer, Neurodegenerative Diseases, and Viral Infections. *J. Med. Chem.* **2020**, *63*, 1892−1907.
(20) Bojkova, D.; et al. Proteomics of SARS-CoV-2-infected host cells reveals therapy targets. *Nature* **2020**, *583*, 469−472.
(21) Skrott, Z.; et al. Alcohol-abuse drug disulfiram targets cancer via p97 segregase adaptor NPL4. *Nature* **2017**, *552*, 194−199.
(22) Pfeffer, G.; Lee, G.; Pontifex, C. S.; Fanganiello, R. D.; Peck, A.; Weihl, C. C.; Kimonis, V. Multisystem Proteinopathy Due to *VCP* Mutations: A Review of Clinical Heterogeneity and Genetic Diagnosis. *Genes* **2022**, *13*, 963.
(23) Banerjee, S.; Bartesaghi, A.; Merk, A.; Rao, P.; Bulfer, S. L.; Yan, Y.; Green, N.; Mroczkowski, B.; Neitz, R. J.; Wipf, P.; Falconieri, V.; Deshaies, R. J.; Milne, J. L. S.; Huryn, D.; Arkin, M.; Subramaniam, S. 2.3 A resolution cryo-EM structure of human p97 and mechanism of allosteric inhibition. *Science* **2016**, *351*, 871−875.
(24) van den Boom, J.; Marini, G.; Meyer, H.; Saibil, H. R. Structural basis of ubiquitin-independent PP1 complex disassembly by p97. *EMBO J.* **2023**, *42*, No. e113110.
(25) Cooney, I.; et al. Structure of the Cdc48 segregase in the act of unfolding an authentic substrate. *Science* **2019**, *365*, 502−505.
(26) Twomey, E. C.; Ji, Z.; Wales, T. E.; Bodnar, N. O.; Ficarro, S. B.; Marto, J. A.; Engen, J. R.; Rapoport, T. A. Substrate processing by the Cdc48 ATPase complex is initiated by ubiquitin unfolding. *Science* **2019**, *365*, aax1033.
(27) van Dun, S.; Ottmann, C.; Milroy, L.-G.; Brunsveld, L. Supramolecular Chemistry Targeting Proteins. *J. Am. Chem. Soc.* **2017**, *139*, 13960−13968.
(28) Fokkens, M.; Schrader, T.; Klärner, F.-G. A Molecular Tweezer for Lysine and Arginine. *J. Am. Chem. Soc.* **2005**, *127*, 14415−14421.
(29) Klärner, F.-G.; Kahlert, B.; Nellesen, A.; Zienau, J.; Ochsenfeld, C.; Schrader, T. Molecular Tweezer and Clip in Aqueous Solution: Unexpected Self-Assembly, Powerful Host-Guest Complex Formation, Quantum Chemical $^{1}$H-NMR Shift Calculation. *J. Am. Chem. Soc.* **2006**, *128*, 4831−4841.
(30) Guillory, X.; Hadrovic, I.; de Vink, P. J.; Sowislok, A.; Brunsveld, L.; Schrader, T.; Ottmann, C. Supramolecular Enhancement of a Natural 14−3-3 Protein Ligand. *J. Am. Chem. Soc.* **2021**, *143*, 13495−13500.
(31) Kitov, P. I.; Sadowska, J. M.; Mulvey, G.; Armstrong, G. D.; Ling, H.; Pannu, N. S.; Read, R. J.; Bundle, D. R. Shiga-like toxins are neutralized by tailored multivalent carbohydrate ligands. *Nature* **2000**, *403*, 669−672.
(32) Mattarella, M.; Garcia-Hartjes, J.; Wennekes, T.; Zuilhof, H.; Siegel, J. S. Nanomolar cholera toxin inhibitors based on symmetrical pentavalent ganglioside GM1os-sym-corannulenes. *Org. Biomol. Chem.* **2013**, *11*, 4333−4339.
(33) Blaskovich, M. A.; Lin, Q.; Delarue, F. L.; Sun, J.; Park, H. S.; Coppola, D.; Hamilton, A. D.; Sebti, S. M. *Nat. Biotechnol.* **2000**, *18*, 1065−1070.
(34) Martos, V.; Bell, S. C.; Santos, E.; Isacoff, E. Y.; Trauner, D.; de Mendoza, J. Calix[4]arene-based conical-shaped ligands for voltage-dependent potassium channels. *Proc. Natl. Acad. Sci. U.S.A.* **2009**, *106*, 10482−10486.
(35) Trads, J. B.; Hüll, K.; Matsuura, B. S.; Laprell, L.; Fehrentz, T.; Görldt, N.; Kozek, K. A.; Weaver, C. D.; Klöcker, N.; Barber, D. M.; Trauner, D. Sign Inversion in Photopharmacology: Incorporation of Cyclic Azobenzenes in Photoswitchable Potassium Channel Blockers and Openers. *Angew. Chem., Int. Ed. Engl.* **2019**, *58*, 15421−15428.
(36) Schrödinger, L.; DeLano, W. *PyMOL*, 2020. Retrieved from. http://www.pymol.org/pymol.
(37) Höing, A.; Kirupakaran, A.; Beuck, C.; Pörschke, M.; Niemeyer, F.; Seiler, T.; Hartmann, L.; Bayer, P.; Schrader, T.; Knauer, S. Recognition of a flexible protein loop in Taspase 1 by multivalent supramolecular tweezers. *Biomacromolecules* **2022**, *23*, 4504−4518.
(38) Meiners, A.; Bäcker, S.; Hadrović, I.; Heid, C.; Beuck, C.; Ruiz-Blanco, Y. B.; Mieres-Perez, J.; Pörschke, M.; Grad, J.-N.; Vallet, C.; Hoffmann, D.; Bayer, P.; Sanchez-Garcia, E.; Schrader, T.; Knauer, S.


https://doi.org/10.1021/jacs.4c15288
J. Am. Chem. Soc. 2025, 147, 16836−16849

Specific inhibition of the Survivin−CRM1 interaction by peptide-modified molecular tweezers. *Nat. Commun.* **2021**, *12*, 1505.
(39) Ding, D.; Li, K.; Liu, B.; Tang, B. Z. Bioprobes Based on AIE Fluorogens. *Acc. Chem. Res.* **2013**, *46*, 2441−2453.
(40) Mei, J.; Leung, N. L. C.; Kwok, R. T. K.; Lam, Y. W. Y.; Tang, B. Z. Aggregation-Induced Emission: Together We Shine, United We Soar. *Chem. Rev.* **2015**, *115*, 11718−11940.
(41) Riebe, S.; Vallet, C.; van der Vight, F.; Gonzalez-Abrado, D.; Wölper, C.; Strassert, C. A.; Jansen, G.; Knauer, S.; Voskuhl, J. Aromatic Thioethers as Novel Luminophores with Aggregation-Induced Fluorescence and Phosphorescence. *Chem.—Eur. J.* **2017**, *23*, 13660−13668.
(42) Stelzer, J.; Vallet, C.; Sowa, A.; Gonzalez-Abradelo, D.; Riebe, S.; Daniliuc, C.; Ehlers, M.; Strassert, C. A.; Knauer, S. K.; Voskuhl, J. On the Influence of Substitution Patterns in Thioether-Based Luminophores with Aggregation-Induced Emission Properties. *ChemistrySelect* **2018**, *3*, 985−991.
(43) Riebe, S.; Wölper, C.; Balszuweit, J.; Hayduk, M.; Ezequiel Gutierrez Suburu, M.; Strassert, C. A.; Doltsinis, N. L.; Voskuhl, J. Understanding the Role of Chalcogens in Ether-Based Luminophores with Aggregation-Induced Fluorescence and Phosphorescence. *ChemPhotoChem.* **2020**, *4*, 398.
(44) Hommel, K.; Kauth, A. M. A.; Kirupakaran, A.; Theisen, S.; Hayduk, M.; Niemeyer, F. C.; Beuck, C.; Zadmard, R.; Bayer, P.; Ravoo, B. J.; Voskuhl, J.; Schrader, T.; Knauer, S. K. Functional Linkers Support Targeting of Multivalent Tweezers to Taspase1. *Chem.—Eur. J.* **2024**, No. e202401542.
(45) The pentamer **133** also shares a $C_6$-symmetric core unit, albeit with one missing arm.
(46) Velazquez-Campoy, A.; Leavitt, S. A.; Freire, E. Characterization of protein-protein interactions by isothermal titration calorimetry. *Methods Mol. Biol.* **2004**, *261*, 35−54.
(47) Fox, J. M.; Zhao, M.; Fink, M. J.; Kang, K.; Whitesides, G. M. The Molecular Origin of Enthalpy/Entropy Compensation in Biomolecular Recognition. *Annu. Rev. Biophys.* **2018**, *47*, 223−250.
(48) van den Boom, J.; Kueck, A. F.; Kravic, B.; Müschenborn, H.; Giesing, M.; Pan, D.; Kaschani, F.; Kaiser, M.; Musacchio, A.; Meyer, H. Targeted substrate loop insertion by VCP/p97 during PP1 complex disassembly. *Nat. Struct. Mol. Biol.* **2021**, *28*, 964−971.
(49) Betts, M. J.; et al. Mechismo - predicting the mechanistic impact of mutations and modifications on molecular interactions. *Nucleic Acids Res.* **2015**, *43*, No. e10.
(50) Rule, C. S.; Patrick, M.; Sandkvist, M. Measuring In Vitro ATPase Activity for Enzymatic Characterization. *J. Vis Exp* **2016**, No. e54305.
(51) Delabarre, B.; Brunger, A. Complete structure of p97/valosin-containing protein reveals communication between nucleotide domains. *Nat. Struct. Biol.* **2003**, *10*, 856−863.
(52) Lescop, E.; Schanda, P.; Brutscher, B. A set of BEST triple-resonance experiments for time-optimized protein resonance assignment. *J. Magn. Reson.* **2007**, *187*, 163−169.
(53) (a) *Desmond Molecular Dynamics System*, D. E. Shaw Research, New York, NY, 2021. (b) *Maestro-Desmond Interoperability Tools*, Schrödinger, New York, NY, 2023.
(54) Jorgensen, W. L.; Tirado-Rives, J. The OPLS [optimized potentials for liquid simulations] potential functions for proteins, energy minimizations for crystals of cyclic peptides and crambin. *J. Am. Chem. Soc.* **1988**, *110*, 1657−1666.
(55) Rostovtsev, V. V.; Green, L. G.; Fokin, V. V.; Sharpless, K. B. *Angew. Chem., Int. Ed.* **2002**, *41*, 2596−2599.
(56) Antonijevic, M.; Rochais, C.; Dallemagne, P. C3-Symmetric Ligands in Drug Design: When the Target Controls the Aesthetics of the Drug. *Molecules* **2023**, *28*, 679.
(57) Höger, S. Shape-Persistent Macrocycles: From Molecules to Materials. *Chem.—Eur. J.* **2004**, *10*, 1320−1329.
(58) Sevlever, F.; Di Bella, J. P.; Ventura, A. C. Discriminating between negative cooperativity and ligand binding to independent sites using pre-equilibrium properties of binding curves. *PLoS Comput. Biol.* **2020**, *16*, No. e1007929.
(59) Kracht, M.; van den Boom, J.; Seiler, J.; Kröning, A.; Kaschani, F.; Kaiser, M.; Meyer, H. Protein Phosphatase-1 Complex Disassembly by p97 is Initiated through Multivalent Recognition of Catalytic and Regulatory Subunits by the p97 SEP-domain Adapters. *J. Mol. Biol.* **2020**, *432*, 6061−6074.
(60) Keller, R. L. *The Computer Aided Resonance Assignment Tutorial*, 1st ed; CANTINA Verlag, 2004.
(61) Madhavi Sastry, G.; Adzhigirey, M.; Day, T.; Annabhimoju, R.; Sherman, W. Protein and ligand preparation: parameters, protocols, and influence on virtual screening enrichments. *J. Comput.-Aided Mol. Des.* **2013**, *27*, 221−234.
(62) Bowers, K. J.; Chow, E.; Xu, H.; Dror, R. O.; Eastwood, M. P.; Gregersen, B. A.; Klepeis, J. L.; Kolossvary, I.; Moraes, M. A., Sacerdoti, F. D.; Salmon, J. K.; Shan, Y.; Shaw, D. E. Scalable algorithms for molecular dynamics simulations on commodity clusters, *Proceedings of the ACM/IEEE Conference on Supercomputing (SC06)*; Tampa, FL, 2006, November 11−17.


https://doi.org/10.1021/jacs.4c15288
J. Am. Chem. Soc. 2025, 147, 16836−16849